AIMS Biophysics

http://www.aimspress.com/journal/biophysics

AIMS Biophysics, 4(3): 400-414.
DOI: 10.3934/biophy.2017.3.400
Received: 30 March 2017
Accepted: 12 June 2017
Published: 20 June 2017

Research article

Cellular deformation characterization of human breast cancer cells under hydrodynamic forces

Ahmad Sohrabi Kashani and Muthukumaran Packirisamy*

Optical-Bio Microsystems Laboratory, Department of Mechanical and Industrial Engineering, Concordia University, 1455 De Maisonneuve Blvd. W. Montreal, Quebec, H3G 1M8, Canada

* **Correspondence:** Email: mpackir@encs.concordia.ca; Tel: +1-514-8482424; Fax: +1-514-848-3175.

Abstract: Understanding how cells sense mechanical forces, and how respond biologically to them is an interesting and quickly-progressing area. Cells within their microenvironment are subjected to various physical forces such as mechanical loads and shear stress. Cells respond and adjust to these forces by mechanotransduction mechanism in which deformation and mechanical forces are converted into biomechanical signals. To quantify mechanotransduction responses and to correctly interpret the behavior of cell under *in vitro* stimulation, magnitude and distribution of the stresses on the cell membrane should be characterized. In this study, a 2D Finite Element Model is introduced to simulate the deformation of individual benign (MCF10A) and malignant (MCF7) human breast cancer cells under hydrodynamic forces. A fluid-structure interaction method is implemented to model fluid flow and the adherent single cells inside a microchannel to study the nature of mechanical forces (viscous and pressure) and to determine their contribution to the deformation of cells. Due to the different mechanical properties, cells respond differently to the forces exerted by the fluid flow. It was found that the maximum stress and strain take place at the interface of the adherent cell and channel wall. Also, under the same boundary conditions, nucleolus and cytoplasm of an individual malignant cell undergo more deformation comparing a single benign cell. Furthermore, it was observed that both two cell lines experience much more stress when their attached area to the substrate is reduced.

Keywords: fluid structure interaction; cellular deformation; human breast cancer cells; biophysical characterization; fluid flow simulation

1. Introduction

Living cells the basic unit of our body have specific biomechanical, bioelectrical, and biochemical properties, allowing them to adopt themselves with their dynamic microenvironment. With the aid of

these biophysical properties, cells are able to preserve their biological functions [1, 2, 3]. In a human body, living cells are constantly subjected to diverse types of biomechanical stimuli particularly fluid dynamic stimuli such as shear and hydrostatic stress. Cells in the human body either are directly exposed to flowing flows or are under a load of interstitial fluid flow arising from the movement of fluid through extracellular matrix of tissue. For example, in the blood vessels, cells such as leukocyte, and epithelial cells are in direct contact with fluid flow and shear stress. However, other types of cells such as bone cells, fibroblasts, muscle cells, human breast cell and articular chondrocytes experience fluid flowing due to deformation of tissues [4, 5, 6]. The shear flow-induced mechanical stress has significant effects on cellular functions of both healthy and cancerous cells such as cell proliferation, transport, gene expression, and apoptosis. For instant, mechanical forces caused by blood flow can affect remodeling and function of vascular endothelial cells, or shear flow can alter viability and proliferation of cancer cells [7, 8]. Mechanotransduction is a mechanism by which cells are able to sense and respond to such bio-mechanical environments by changing their morphology of membrane or their rigidities. With the help of this mechanism, cells convert deformation caused by mechanical forces into biological signals in order to adjust themselves to the changes. The reaction of cells in the form of morphological and functional responses not only help cells to maintain their physiological functions but also play a significant role in development and progresion of diseases such as cancer and metastasis [9, 10]. How cells respond to the mechanical stress is conditional to both specific molecular sensors, and their internal mechanical properties. Mechanical properties of single living cells change in accordance with their healthy level. For example, many studies have substantiated that metastasis cancer cells are less stiff comparing to normal or benign cells [11, 12]. Due to different mechanical properties of normal and cancerous cells, they respond differently to the fluid flows in the body. So, further research on such different cellular responses of healthy and unhealthy cells could provide a possible method for diagnosis of diseases.

Due to the difficulty of controlling hydrodynamic conditions under *in vivo* studies, an isolated cultured cells under well-defined conditions need to be studied to investigate the responses of cells to the hydrodynamic stimuli. Owing to the complex geometry of cells, complex boundary conditions, and inhomogeneous nature of cells, with cell experimentations alone, the response of single cells to fluid flow cannot be interpreted clearly [3]. Computational models not only enable us to interpret the experimental results but also provide us ability to predict the response of cells to their biomechanical environment. Many experimental and computational analyses have been made to understand how living cells respond to the fluid flow inside a human body. McGarry et al. [13] computationally and experimentally studied the deformation of bone cells under shear stress using solid mechanic model. Aleksey Ni et al. [14] developed a 2D model to study the motion and deformation of a single red blood cell (RBC) under different flow conditions in a micro-capillary filled with plasma alcohol using finite element method (FEM). Michael C et al. [15] applied computational method to estimate heterogeneous displacement and stress-strain field in sheared and focally adherent endothelial cells. Moreover, it has been substantiated that surface tension can affect the mechanical responses of the biological cells [16], and its effect has been studied computationally. For instant, Ding et al. [17] used FEM to study the effects of surface tension on the mechanical responses of the living cells. They showed that by considering the surface tension effects, the elastic modules of living cells can be interpreted with higher accuracy when they are probed by Atomic Force Microscopy (AFM).

In this study, we developed a fluid-structure interaction model in order to characterize the

deformation of adherent benign human breast cancer cell (MCF 10A) and malignant human breast cancer cell (MCF7) under the action of hydrodynamic fluid flow. Cells experience different stress, strain and deformation when they are subjected to hydrodynamic forces with respect to their mechanical properties. It is well-known that elastic properties of cancerous and normal are different, and cancerous cells are softer comparing their counterpart [10]. Therefore, when they are subjected to the hydrodynamic stimuli, they exhibit different deformations. To the best of our knowledge, cellular deformation comparison between cancerous and healthy cells exposing to hydrodynamic stimuli have not been studied computationally. This study is presented to compare deformations and responses of both cell lines under the same conditions. This study not only could help us to fully understand mechanotransduction mechanisms of healthy and cancerous cells, but also enable us to characterize the behavior of human breast cells in various healthy levels under *in vitro* mechanical stimuli.

2. Materials and Methods

2.1. Fluid structure interaction model

The main objective of this project is to characterize fluid flow parameters within a microchannel and quantify mechanical stresses acting on the healthy and cancerous cells due to the hydrodynamic forces. With the aid of this numerical study, the cellular deformation of normal and cancerous human breast cancer cells is also computed under the applied fluid flow regime. A schematic of the channel under the investigation in this computational study and the adherent cells are shown in Figure 1 . The channel includes two parallel plates, and the target cell is attached on the bottom plate. This parallel-plate flow chamber is used to incite the attached cells by creating a pressure gradient across the microchannel [18]. Fluid flow within channel imposes both shear and normal mechanical stresses at the interface of cell surfaces and surrounding fluid flow. Cellular deformations and the presence of cells themselves affect fluid flow within the channel. The interaction of cells and surrounding fluid flow either can be weakly coupled in one-way method or strongly coupled in two-way method [19]. In the one-way method, it is assumed that the deformation of cells is relatively low, so the effects of changes in the solid domain on the fluid domain are ignorable. However, in two-way coupling, the fluid flow parameters are influenced by changes in solid domain or deformation of cells.

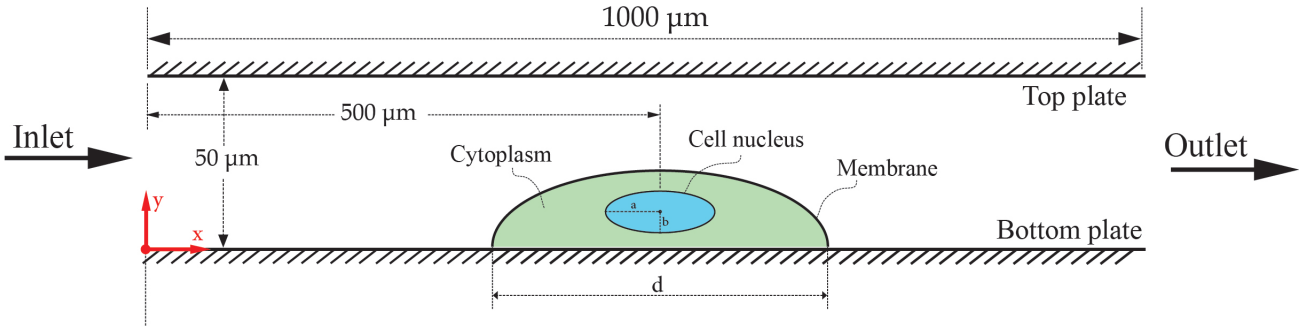

Figure 1. Schematic of an adherent cell within a channel (*d*: diameter of the cell).

2.2. Case study and governing equations

The system includes a main microchannel with one inlet, one outlet and an adherent cell on the bottom plate of the main channel. A 2D numerical analysis is carried out in order to estimate the flow parameters within the main microchannel as well as characterize deformation of cells under various inlet flow rates. The strongly coupled method is used to numerically solve the interactions between the surrounding fluid and the cell domain. The fluid flow in the microfluidic system is assumed to be Newtonian, laminar, viscous and incompressible flow. The motion of an incompressible Newtonian flow is expressed by Navier-Stokes and continuity equations as follows [20]:

$$\rho\frac{\partial u}{\partial t} - \nabla(-pI + \mu(\nabla u + (\nabla u)^T) + \rho(u.\nabla).u) = F \tag{1}$$

$$\nabla .(u) = 0 \tag{2}$$

Where ρ is the density of fluid, p is the fluid pressure, u is the velocity field inside the microchannel, t the time, $\nabla()$ the divergence operator, I is unit diagonal matrix, μ the fluid dynamic viscosity and F is the affecting force on the fluid. For a fluid flow without gravitation and other volume forces, the volume body force can be ignored ($F = 0$). The total hydrodynamic loads acting on the surface of cells are defined as forces per area as follow [21]:

$$F^T = -n. \triangle (-pI + \mu(\triangle u + (\triangle u)^T)) \tag{3}$$

Where n is the outward normal unit vector of the boundary, u is the velocity field on the surface of cells pointing out from fluid. F^T is the fluid loading including pressure and viscous forces. The first term in equation (3) is the pressure gradient which is extracted from the fluidic simulation results. The second term is the viscous component of the force which is a function of velocity and dynamic viscosity of the fluid. On the fluid-cell interface the fluid velocity equals the rate of change of the cell, and this interface is considered as no-slip wall for the fluid domain. In order to have laminar fully developed flow at the local area of the adherent cell, the test section in our simulation were designed to be longer than expected hydrodynamic entry length. Entry length correlating with Reynold number(Re) can be obtained by $Le = 0.006Re.D$. Reynold number within microchannel region for all flow regime is defined as follow:

$$Re = \frac{\rho v D}{\mu} \tag{4}$$

Where v is the mean velocity, D is the hydraulic diameter of the channel, and μ is dynamic viscosity of the fluid.

2.3. Material properties

In the present work, the cell is modeled as an oblate-shape body having cytoplasm and nucleus, and the cell is separated from the surrounding environment by a membrane. An ellipsoidal shape is assumed for the nucleus of the cells to estimate their behavior and deformation. Both cytoplasm and nucleus of the cell are modeled as hyperelastic material, and it is assumed that the adherent cell has isotropic and homogeneous material properties. Table 1 shows dimensions and material properties of human breast cell lines which were used in the finite element modeling [12, 22, 23]. As mentioned

above, the mechanical properties of the two cells lines are different, and the Young module of MCF7 is smaller comparing benign human breast cells. Hence, these differences were taken into account in our simulation by using different values for both cells. Young module values available in literature for MCF10A and MCF7 vary from 0.25 the kPa to 0.7 kPa, and from 0.15 kPa to 0.47 kPa respectively; 0.47 kPa and 0.7 kPa were chosen for MCF10A and MCF7 cells, respectively as the maximum values to perform simulation. Nucleus stiffness is greater than cytoplasm region, and based on the information available in the literature, the stiffness of nucleus was considered ten times greater than the stiffness of cytoplasm [24, 25]. The fluid medium is assumed to be an incompressible Newtonian fluid having properties as same as water. Dynamic viscosity of 0.001 pa.s and density of 997 kg/m^3 were used as the properties of water in our analysis, and no-slip condition was considered for both top and bottom plates.

Table 1. Dimensions and material properties of human breast cell lines.

Parameters (unit)	MCF 7	MCF 10 A
Average diameter (μm) [12, 23]	$d = 12$	$d = 14$
Nucleus size-ellipsoidal shape (μm) [12]	$a = 3.2, b = 1$ (*)	$a = 2.8, b = 1$
Height of profile (μm) [12]	3.15	3.3
Elasticity of cytoplasm (kPa) [25]	0.47	0.7
Elasticity of Nucleus (kPa) [24, 25]	4.7	7.0
Density of Cytoplasm (gr/cm^3) [25]	1.05	1.05
Density of Nucleus (gr/cm^3) [25]	1.3	1.3
Poisson's ratio [22, 25]	0.49	0.49

(*) *a: half of major diameter, b: half of minor diameter.*

2.4. Numerical Simulation

In order to solve governing equation as well as modeling microchannel, cell and fluid flow within microchannel, a commercial software for finite element analysis known as COMOSL Multiphysics 5.2 was used. To have fully coupled solver, a 2D model with moving mesh modules was utilized to model the interaction between fluid and the cell. The fluid flow domain changes considerably by deformation of the solid domain (cell), so in order to couple the solid and fluid domain together, a direct two-way coupling formulation was implemented. Simulation with different velocities and boundary conditions were performed to induce various external shear stresses on the surface of the cell, and to distinguish the different behaviors of normal and cancerous cells. An iterative, segregated solution method was used to carry out all simulations. In order to obtain a converged solution, the variables were solved repeatedly and sequentially. Mesh element of the system including cell and surrounding fluid flow is shown in Figure 2A. The size of elements inside the cell and at the interface of cell and fluid flow are smaller than other parts of the domain to have reasonable accuracy for very small changes. Figure 2B presents streamlines and magnitude of velocity neighboring the cells. From this figure, it is evident that streamlines closing to the cells are influenced by the body of the attached cells.

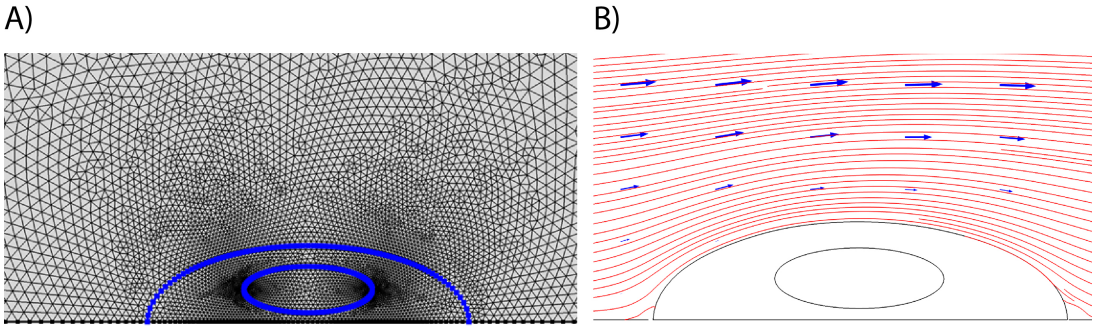

Figure 2. (A) Mesh network and elements sizes for system of an adherent cell (MCF10A) and fluid flow; (B) Stream lines around the cell (arrows illustrates the direction and magnitude of velocity within the channel).

3. Results and Discussion

Using the design in Figure 1, dimensions and material properties shown in Table1, fluid flow were simulated within the microchannel to characterize flow parameters. Before deriving the results, a mesh independence test was performed to choose an appropriate mesh size in accordance with the size of the channel and the adherent cell. The pressure along the length of microchannel at the local area of the cells was computed by decreasing mesh size and increasing degree of freedom. Properties of various mesh element sizes used in the simulation are shown in Table 2. This process performed until reaching ignorable differences between the results for two successive mesh size. The pressure along microchannel is plotted in Figure 3 under various mesh elements sizes. Based on the result, the difference between mesh 3 and 4 is very small, so in order to have efficient computation, the mesh 3 was used for the following simulation.

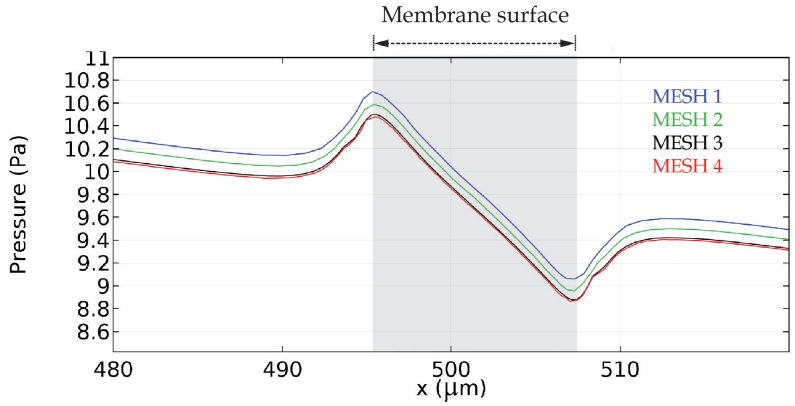

Figure 3. Pressure along length of bottom wall and membrane surface of an adherent cell under various mesh sizes.

Table 2. Properties of elements in various mesh types.

Mesh number	Maximum element size (μm)	Minimum element size (μm)	Grow rate	Curvature factor	Resolution of curvature	Number of elements
Mesh 1	37	0.125	1.26	0.3	1	1604
Mesh 2	20	0.075	1.2	0.26	1	2413
Mesh 3	5	0.02	1.12	0.24	1	10822
Mesh 4	3	0.01	1.08	0.2	1	21359

Figure 4 compares pressure fields within the microchannel for two different conditions: when the channel is free (without cell), and when it is occupied by either MCF7 or MCF10A cell lines. This figure clearly demonstrates the effect of solid domain (the adherent cell) on the pressure field at the zone of a single cell. For the free channel, pressure along the length of the channel is linearly decreased, while for a channel with the cell, a variation in pressure near the cell is observable. Similarly, any changes at the boundary of the cell such as membrane deformation can alter flow parameters such as velocity and pressure within the channel. The deformable structure of the cell deforms when it is subjected to a pressure, and as a return, this deformation changes the flow field.

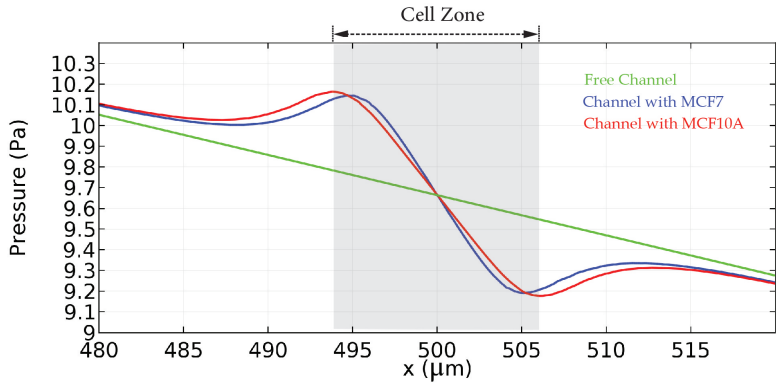

Figure 4. Pressure along channel for three various conditions: free channel, channel with cancer cell and channel with healthy cell.

Figure 5 indicates the contour of Von Mises stresses for two different cell lines and corresponding shear stress along the channel and in the vicinity of cells. As mentioned in Section 2.2 and Equation 3, forces acting on the membrane of the cells include both viscous and pressure forces. For a steady, laminar and fully developed flow between two infinite stationary plates, the shear stress within flow field can be obtained using the following expression [20]:

$$\tau_{yx} = \frac{6\mu U_{ave}}{h}\left\{1 - 2\frac{y}{h}\right\} \tag{5}$$

Where μ is dynamic viscosity of fluid, U_{ave} presents average velocity, h is height of channel and y is distance from bottom plate. For an inlet average velocity of 4 mm/s, imposing shear stress on the wall of bottom plate ($y = 0$) of the system is $\tau_0 = 0.48\ Pa$ using Equation 5. Figure 5 shows that shear

stress on the bottom wall is constant along the channel and is matched with the analytical solution (using Equation 5) except in the inlet, outlet of the channel and the local area of cell. In the vicinity of the cell, the shear stress on the membrane of the cell is significantly increased due to the existence of the cells. The results indicate that the shear stresses on the membrane of the cells are almost two times greater than shear stress on the wall. From the contours, it is evident that maximum stress takes place at the interface of cell and substrate, the minimum stress is at the interface of cytoplasm and nucleus. Since the cancerous cells are softer, cytoplasm and nucleolus of them undergo more deformation under same hydrodynamic loading compared to MCF10A cell lines.The effect of hydrodynamic load on the nucleus of MCF10A is less in comparison to MCF7, it means that greater force is transferred from membrane of MCF7 to its nucleus.

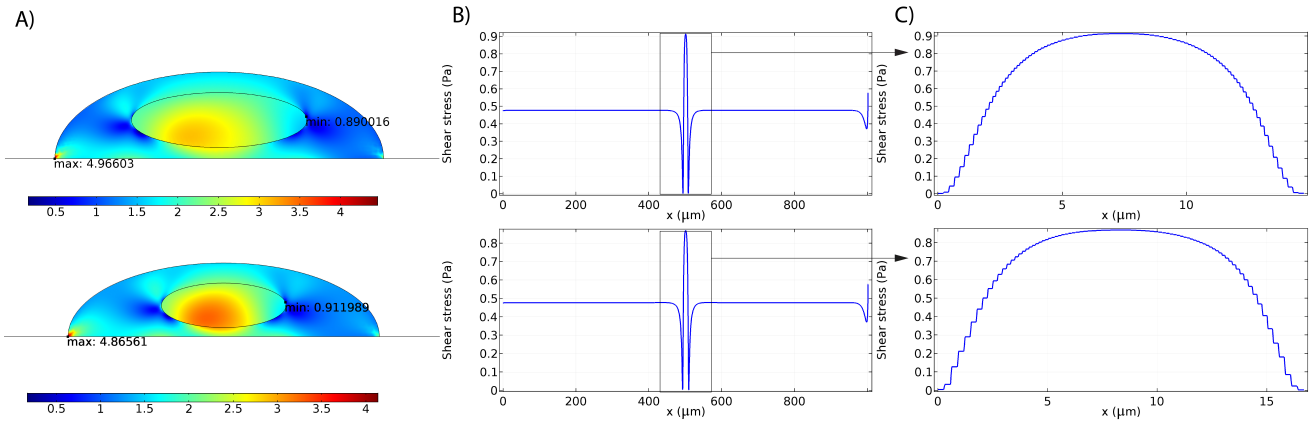

Figure 5. Von Mises stresses (A) over two cell types and corresponding shear stress along length of the channel; (B) and membrane surface; (C) of the adherent cells under inlet average velocity of 4 mm/s.

To study the effect of fluid flow on the cell lines and quantify their deformation, cellular deformation of the cells under various inlet velocities were computed using equivalent elastic strain (EQS). Von Mises equation can be used to define EQS for elastic material as follows [26, 27]:

$$EQS = \frac{1}{\sqrt{2}(1+\nu)}\left\{(\varepsilon_{xx}-\varepsilon_{yy})^2+(\varepsilon_{zz}-\varepsilon_{yy})^2+(\varepsilon_{xx}-\varepsilon_{zz})^2\right\}^{\frac{1}{2}} \tag{6}$$

Where ν is Possion's ratio, ε_{xx} , ε_{yy} and ε_{zz} are principal strains in direction of x, y and z respectively. Figure 6 shows contours of equivalent elastic strains for the two cell lines when they are subjected to various hydrodynamic forces due to different average inlet velocities. It was assumed that the cell is completely attached to the bottom plate, so that no displacement happens at substrate-cell interface. It can be seen in this figure that greater values of EQS occur in regions between substrate-cell interface and nucleus of each cell types. As it was observed from Figure 5, cells experience maximum value of shear stress at the top of membrane, and hence the EQS values are greater comparing other parts of the cell at these regions. Moreover, these results show the effect of hydrodynamic force on the deformation of nucleus under various inlet velocities. Even though nucleus of cells are stiffer, by increasing the inlet velocity, more deformation is experienced by nucleus of each cell lines. As expected, nucleus of MCF7 lines are deformed much more at the same inlet velocity when compared to MCF10A lines due

to its lower stiffness. It means that nucleolus of malignant cells senses more deformation under same mechanical forces within channel.To characterize the deformation values for cytoplasm and nucleus of the two cell types, the average equivalent elastic strain (AEQS) for nucleus and cytoplasm of each cell lines were computed by averaging EQS over nucleus and cytoplasm surfaces of the both cells. The average equivalent elastic strains are shown in Figure 7 for different inlet average velocities. The result shows that average EQSs for MCF7 are approximately 1.4 and 1.5 times greater than MCF10A for cytoplasm and nucleus respectively. Hence, hydrodynamic forces which are transmitted through the cells of MCF7 are much more at the same conditions in comparison to another cell line. It can been seen from this figure that average equivalent elastic strain is increased with respect to inlet average velocities.

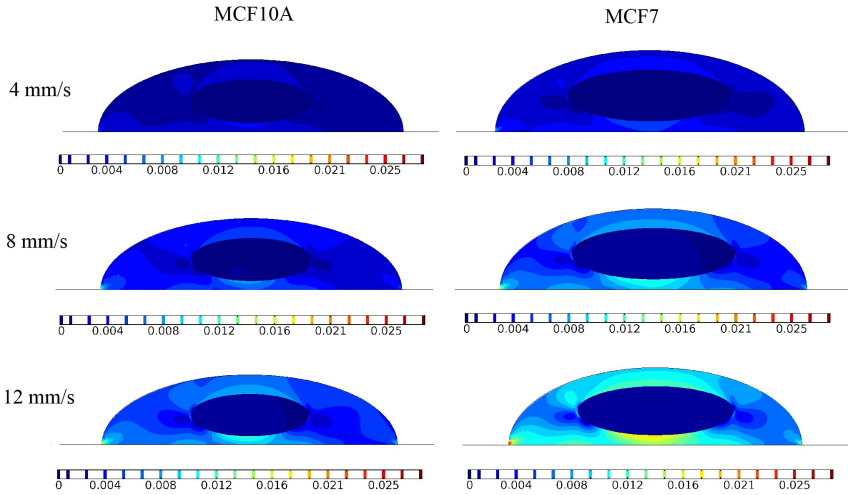

Figure 6. Distribution of equivalent elastic strain (EQS) for both MCF10A and MCF7 under various average inlet velocities: 4 mm/s, 8 mm/s and 12 mm/s.

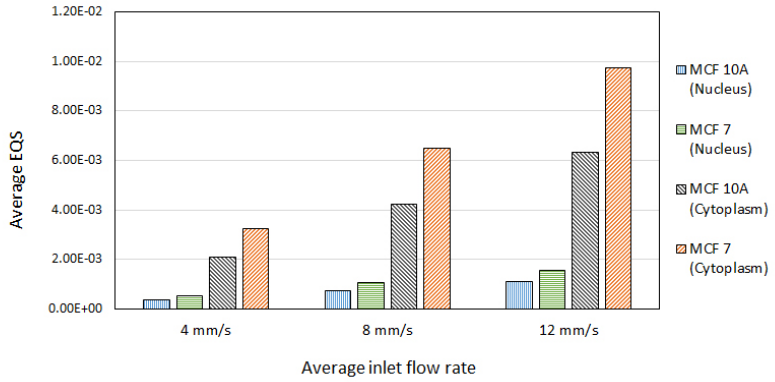

Figure 7. Average equivalent elastic strain (EQS) over nucleus and cytoplasm of the cells under different average inlet velocities.

As mentioned in Equation 3, total forces acting on the membrane of the cell is a combination of viscous and pressure forces. Due to different pressure between the surfaces of fluid flow, the pressure

gradient force is produced, while due to friction between layers of fluid flow, the viscous forces is produced in the opposite direction of flow. Deformation of cells does not determine the contribution of each forces to the total force, so it would be useful if we can quantify the contribution of each forces to the total forces acting on the cells. Figure 8 illustrates the amplitude and direction of pressure and viscous forces applying to the adherent cell under fluid flow inside microchannel. Viscous forces are tangent to the fluid-cell interface boundary, and it is clear that the maximum forces due to viscosity is applied at the top of cell, and its values are decreased significantly by moving toward the sides of the cells. The length of the arrows at different points express the amplitude of forces at those points. Pressure forces are normal to the fluid- cell interface boundary, and its values are more uniform comparing with the viscous forces. Figure 9 compares the values of total viscous and pressure forces along both MCF7 and MCF10A cells. It is evident that pressure forces are much greater in comparison with viscous forces, so their contribution to the deformation of cells would be more significant. For the setting boundary conditions and the geometry of channel, the pressure forces are more than ten times than viscous forces. These results emphasize the significant role of pressure on the deformation of cells compared to viscous forces. Figure 9 also highlights the different magnitude of loads arising from pressure forces acting on the membrane of the cells compared to the viscous forces under different inlet velocities. By increasing the average inlet velocity, both total pressure and total viscous forces are increased, but due to more contact area between MCF10A and surrounding fluid flow, they are subjected to more forces in comparison to the MCF7 cells.

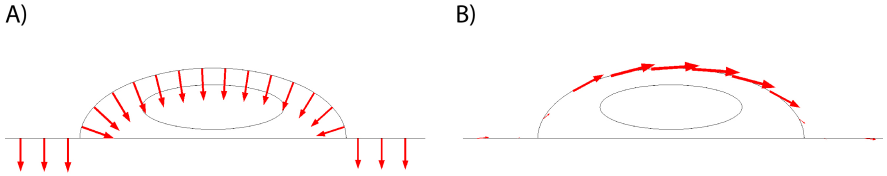

Figure 8. Pressure and viscous forces (arrows are proportional to the magnitude of forces at the indicated points). (A) Pressure force acting on the membrane of cell; (B) Viscous force acting on the membrane of cell (the scales of arrows for pressure and viscous forces are not identical).

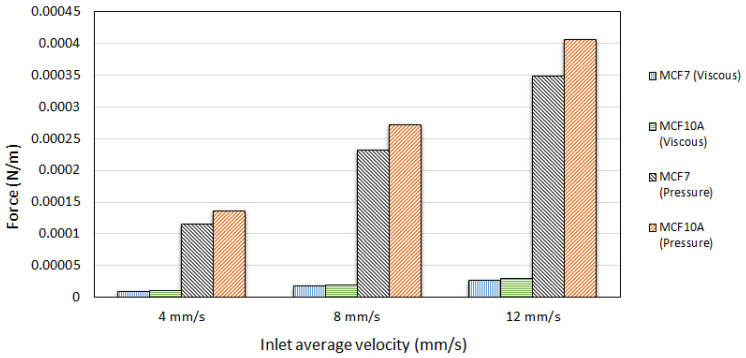

Figure 9. Total pressure and total viscous forces acting on the membrane of two cell lines under various average inlet velocities.

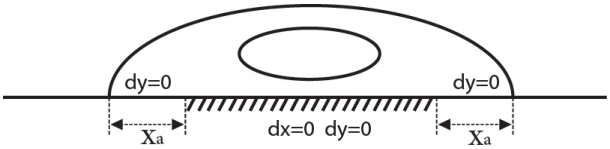

Figure 10. Schematic of fixation of cell to the substrate.

Due to reduced cell surface adhesion molecules in cancerous cells, most of them are less adhesive compared to their normal counterparts. As a result, cancer cells are not restrained completely by interaction with tissue components or their substrate, giving them the ability to invade and metastasize. Reduced adhesiveness to the substrate causes morphological and cytoskeletal changes of cancerous cells, so they are rounder than normal cells [28, 29]. For previously obtained results, it was assumed that cell attaches to the substrate completely, so there is no deflection at the interface of cell and substrate. In order to study the effects of adhesion on the deformation of cells and mimic their microenvironment, the simulation were performed assuming that cells partially adhere to the substrate so that cells are free to deform at the two sides in x- direction only while still they are fixed in y-direction. Figure 10 illustrate how cells were constrained on their cell-substrate interface for the simulation by considering various attached areas. As this figure shows, there is no deflection for the center of cell. However, at x_a distance away from two ends, it can be deformed only in x direction.

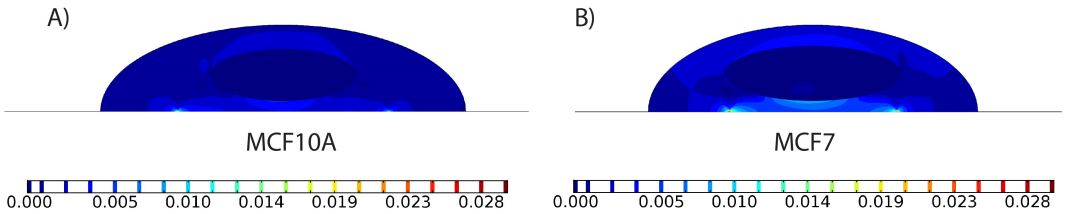

Figure 11. EQS contours when cells are adhered partially ($x_a = 3\ \mu m$). (A) MCF10A, (B) MCF7 (inlet average velocity: 4 mm/s).

To study the effect of x_a, the average equivalent elastic strains of the two cell lines were computed for different values of x_a, and the results are shown in Figure 11 and Figure 12. The average EQS increases by increasing the x_a, but the increase in deformation is not similar for both cytoplasm and nucleolus of two cell lines. Figure 12B compares the increased percentage in EQS with respect to the x_a. This figure clearly demonstrates that the nucleolus EQS of the cell under constant inlet average velocity is influenced more by increasing x_a compared to the cytoplasms. Due to shorter attached area of cells to the bottom plate, more stresses are experienced by them under same boundary conditions. It was shown that the maximum stresses occurs on the cell-substrate interface, and the maximum value of stress were measured to understand the effect of various attached areas on it. Figure 13 shows the maximum stress estimated in two cell lines when x_a changes from 0 to 4 μm. The maximum stress can be increased from 5 Pa when $x_a = 0$ to 15 Pa when $x_a = 4$ for MCF7 cells.

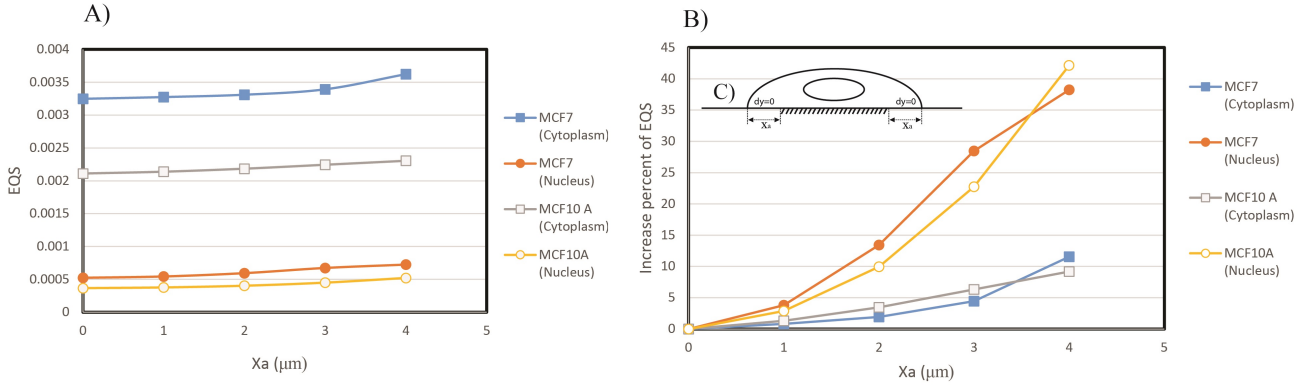

Figure 12. (A) Average EQS for cytoplasm and nuclues of both cell lines versus different x_a as shown in (C); (B) Increased percentage of EQS versus different x_a compared with EQS of two cell lines when $x_a = 0$ (inlet average velocity: 4 mm/s).

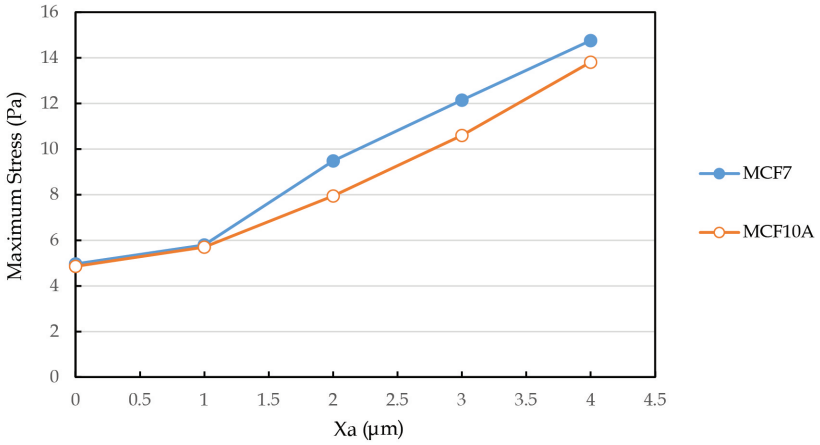

Figure 13. Maximum stress estimated in the two cell lines for different x_a (inlet average velocity: 4 mm/s).

4. Conclusions

Biological function of cells and their behavior are affected by biomechanical forces such as shear stress in their environmentt. These mechanical stimulations can also alter phenotype of those cells. Cells respond to fluid shear stresses by mechanotransduction mechanism, and they exhibit various deformations with respect to their mechanical properties such as elasticity and density. In this study, a fluid-structure interaction model was developed to quantify deformation of both normal and cancerous cells under flow-induced hydrodynamic loads including viscous and pressure forces. It was observed that the maximum stresses take place at cell-substrate and the minimum at cytoplasm- nucleolus interface. The obtained results show that nucleus and cytoplasm of MCF7 cancer cells undergo almost one and half times more deformation than MCF10A benign cells under the same conditions. To differentiate the effects of viscous and pressure forces individually on the deformation of cells, the

contribution of each forces was estimated numerically. The adherent cells undergo the hydrodynamic force which is a combination of pressure and viscous forces, but our numerical study reveals that the imposing total pressure on the membrane of the cells due to flow field, is much more (ten times greater) than total viscous forces within channel. It suggests that the pressure field provides a major contribution to the deformation of the adherent cells. Moreover, the FSI model was used to study the effect of partial adhesion of the cells on the their deformation. By the reducing the cell adhesion, the deformations of both MCF10A and MCF7 increased under the constant inlet velocity, but the amount of increase is not identical for both cytoplasm and nucleus. When the cell adhesion was reduced, the physical deformation of cell increased considerably in response to forces. This study can provide a useful insight on the behavior of individual cancerous and normal cells under flow conditions.

Acknowledgments

We would like to acknowledge NSERC-Discovery (Natural Sciences and Engineering Research Council of Canada), FQRNT-Team (Fonds Québécois de la Recherche sur la Nature et les Technologies) and CURC (Concordia Research chair) research grants of MP.

Conflict of Interest

The authors declares no conflicts of interest in this paper.

References

1. Zheng Y, Nguyen J, Wei Y, et al. (2013) Recent advances in microfluidic techniques for single-cell biophysical characterization. *Lab Chip* 13: 2464–2483.
2. Kim DH, Wong PK, Park J, et al. (2009) Microengineered platforms for cell mechanobiology. *Annu Rev Biomed Eng* 11: 203–233.
3. Rodriguez ML, McGarry PJ, Sniadecki NJ (2013) Review on cell mechanics: experimental and modeling approaches. *Appl Mech Rev* 65: 060801.
4. Sakamoto N (2014) Responses of Living Cells to Hydrodynamic Stimuli Due to Fluid Flow, In: *Visualization and Simulation of Complex Flows in Biomedical Engineering*, Springer Netherlands, 165–180.
5. Yao W, Ding GH (2011) Interstitial fluid flow: simulation of mechanical environment of cells in the interosseous membrane. *Acta Mech Sin* 27: 602–610.
6. Brindley D, Moorthy K, Lee JH, et al. (2011) Bioprocess forces and their impact on cell behavior: implications for bone regeneration therapy. *J Tissue Eng* 620247.
7. Fan R, Emery T, Zhang Y, et al. (2016) Circulatory shear flow alters the viability and proliferation of circulating colon cancer cells. *Sci Rep* 6.
8. Wang J, Heo J, Hua SZ (2010) Spatially resolved shear distribution in microfluidic chip for studying force transduction mechanisms in cells. *Lab Chip* 10: 235–239.
9. Shemesh J, Jalilian I, Shi A, et al. (2015) Flow-induced stress on adherent cells in microfluidic devices. *Lab Chip* 15: 4114–4127.

10. Lee GY, Lim CT (2007) Biomechanics approaches to studying human diseases. *Trends Biotechnol* 25: 111–118.
11. Hou HW, Lee WC, Leong MC, et al. (2011) Microfluidics for applications in cell mechanics and mechanobiology. *Cell Mol Bioeng* 4: 591–602.
12. Corbin EA, Kong F, Lim CT, et al. (2015) Biophysical properties of human breast cancer cells measured using silicon MEMS resonators and atomic force microscopy. *Lab Chip* 15: 839–847.
13. McGarry JG, Klein-Nulend J, Mullender MG, et al. (2005) A comparison of strain and fluid shear stress in stimulating bone cell responses—a computational and experimental study. *FASEB J* 19: 482–484.
14. Ni A, Cheema TA, Park CW (2015) Numerical Study of RBC Motion and Deformation through Microcapillary in Alcohol Plasma Solution. *Open J Fluid Dyn* 5: 26.
15. Mitchell MJ, King MR (2013) Computational and experimental models of cancer cell response to fluid shear stress. *Front Oncol* 3: 44.
16. Ramsey F, Cathie P, Gabor F, et al. (1996) Surface tensions of embryonic tissues predict their mutual envelopment behavior. *The Company of Biologists Ltd* 122: 1611–1620
17. Ding Y , Xu GK , Wang GF (2017) On the determination of elastic moduli of cells by AFM based indentation. *Sci Rep* 7.
18. Brown TD (2000) Techniques for mechanical stimulation of cells in vitro: a review. *J Biomech* 33: 3–14.
19. Benra FK, Dohmen HJ, Pei J, et al. (2011) A comparison of one-way and two-way coupling methods for numerical analysis of fluid-structure interactions. *J Appl Math* 2011.
20. Bruus H (2008) Theoretical microfluidics, Springer Netherlands, 165–180.
21. Basak S, Raman A, Garimella SV (2006) Hydrodynamic loading of microcantilevers vibrating in viscous fluids *J Appl Phys* 99: 114906.
22. Guck J, Schinkinger S, Lincoln B, et al. (2005) Optical deformability as an inherent cell marker for testing malignant transformation and metastatic competence. *Biophys J* 88: 3689–3698.
23. Liu Z, Lee Y, hee Jang J, et al. (2015) Microfluidic cytometric analysis of cancer cell transportability and invasiveness. *Sci Rep* 5: 14272.
24. Caille N, Thoumine O, Tardy Y, et al. (2002) Contribution of the nucleus to the mechanical properties of endothelial cells. *J Biomech* 35: 177–178.
25. Geltmeier A, Rinner B, Bade D, et al. (2015) Characterization of dynamic behaviour of MCF7 and MCF10A cells in ultrasonic field using modal and harmonic analyses. *PloS one* 10: e0134999.
26. SAS I (2012) ANSYS Mechanical APDL Theory Reference.
27. Vaughan TJ, Mullen CA, Verbruggen SW, et al. (2015) Bone cell mechanosensation of fluid flow stimulation: a fluid-structure interaction model characterising the role integrin attachments and primary cilia. *Biomech Model Mechanobiol* 14: 703–718.
28. Cooper GM, Hausman RE (2000) The cell. *Sinauer Associates* 725–730.
29. Martin TA, Ye L, Sanders AJ, et al. (2013) Cancer invasion and metastasis: molecular and cellular perspective. *Landes Bioscience*.

AIMS Press